Doi:10.1038/nnano.2008.7

Classification and control of the origin of photoluminescence from Si nanocrystals

S. Godefroo[1], M. Hayne[1,2*], M. Jivanescu[3], A. Stesmans[3], M. Zacharias[4], O. I. Lebedev[5], G. Van Tendeloo[5] and V. V. Moshchalkov[1]

[1] INPAC-Institute for Nanoscale Physics and Chemistry, Pulsed Field Group, K.U.Leuven, Celestijnenlaan 200 D, B-3001 Leuven, Belgium

[2] Department of Physics, Lancaster University, Lancaster LA1 4YB, United Kingdom

[3] INPAC-Institute for Nanoscale Physics and Chemistry, Semiconductor Physics Laboratory, K.U.Leuven, Celestijnenlaan 200 D, B-3001 Leuven, Belgium

[4] Institute of Microsystems Engineering, Albert Ludwigs University Freiburg, D-79110 Freiburg, Germany

[5] EMAT, University of Antwerp (RUCA), Groenenborgerlaan 171, 2020 Antwerp, Belgium

*e-mail: m.hayne@lancaster.ac.uk

Doi:10.1038/nnano.2008.7

Abstract

Silicon dominates the electronics industry, but its poor optical properties mean that III-V compound semiconductors are preferred for photonics applications. Photoluminescence at visible wavelengths was observed from porous Si at room temperature in 1990, but the origin of these photons - highly-localized defect states or quantum confinement effects? - has been the subject of intense debate ever since. Since then attention has shifted from porous Si to Si nanocrystals, but the same fundamental question about the origin of the photoluminescence has remained. Here we show, based on measurements in high magnetic fields, that defects are the dominant source of light from Si nanocrystals. Moreover, we show that it is possible to control the origin of the photoluminescence in a single sample: passivation with hydrogen removes the defects, resulting in photoluminescence from quantum-confined states, but subsequent UV illumination reintroduces the defects, making them the origin of the light again.

Doi:10.1038/nnano.2008.7

INTRODUCTION

For all its success as an electronic material, silicon has one major disadvantage: an indirect band-gap that makes it a poor light-emitter. This has given the information age a 'split personality'[1], in which digital data processing is performed by Si electronics, but increasingly vast amounts of data are transferred optically using photons generated and detected by III-V semiconductors. This problem is likely to become more acute in the near future as the information technology industry moves to optical interconnects for board to board and chip to chip communications.

The discovery of room-temperature visible photoluminescence (PL) from porous Si in 1990[2,3] increased interest in the optical properties of Si and opened a long-running debate on the origin of PL from porous Si[4,5] and, more recently, from Si nanocrystals embedded in SiO_2[6,7,8,9,10,11]. Besides their potential as light sources[12,13], it has been shown that Si nanocrystals are strong candidates for a new generation of Flash memory that can be fabricated with minimal disruption to conventional silicon technology[14].

A consensus has been reached that highly-localised defects at the Si/SiO_2 interface[8,9,10] and the quantum confinement of excitons[15,16,17] both play important roles, but it is difficult to experimentally distinguish the mechanisms in the radiative emission[9,10], especially since the interface-related PL depends on nanocrystal size[8,9,10,11]. Here, we report the use of high-field magneto-PL ($\leq$50 T) experiments to directly probe the extent of the wave function responsible for the PL[18,19], and demonstrate that the PL is dominated by defect states. Our results are corroborated by performing electron spin resonance (ESR) measurements which are used to monitor the presence or absence of (paramagnetic) defects in the sample.[20] We also show that the origin of the PL can be controlled, by using hydrogen passivation to remove the defects, resulting in PL that is due to quantum confinement, and UV illumination to re-introduce them.

Doi:10.1038/nnano.2008.7

Si/SiO_2 NANOCRYSTALS AND THEIR DEFECTS

The sample consists of Si nanocrystals embedded in SiO_2, and was grown by the deposition of a SiO/SiO_2 superlattice on a Si substrate and subsequent formation of Si nanocrystals in the SiO layers via annealing[21]. Transmission electron microscopy (TEM) images show that the annealed sample discussed here consists of 37 bi-layers with thicknesses of 1.5 nm for the layer containing the nanocrystals and 3 nm for the SiO_2 layers. High-resolution TEM shows that the nanocrystals have an in plane diameter of around 3 nm. Most particles are oblate with a reduced dimension (~1.5 nm) perpendicular to the layers; whilst others are facetted by (111) planes (Fig.1). The images clearly show a crystalline Si core (Fig. 1), and this is supported by our ESR data, as well as by previous soft x-ray spectroscopy on similar samples[22]. Less comprehensive experiments were also conducted on five other samples, and gave results that are consistent with those reported here. In particular, it should be noted that the origin of the PL in the as-crystallised state, as determined by magneto-PL, was usually found to be defect-related, but was sometimes QC. This variation amongst samples correlated with the defect-densities measured using ESR.

The room-temperature PL of the sample in its as-crystallized state is shown in Fig. 2. It consists of a broad Gaussian peak centred at 1.61 eV, and is typical of PL from Si nanocrystals. In order to establish the origin of the PL two types of experiments were conducted on the sample: ESR and magneto-PL. In the first instance, a high-sensitivity ESR analysis was applied to the sample to quantify the presence of any paramagnetic defects. Two different defect centers are identified (upper spectrum in Fig. 3): $P_{b(0)}$[23] and P_{b1}[24]. These defects are prototype interface defects characteristic of the Si/SiO_2 interface and are schematically represented in Fig. 3. The presence of P_b-type defects is important, as these are deep non-radiative recombination centres, which are known to quench the PL from Si nanocrystals in the 1.4-2.2 eV range[15], irrespective of whether the source of the PL is

quantum confinement or interface states. The absence of any angle dependence in the P_b ESR signal indicates that these defects must stem from the interface between the Si nanocrystals and the surrounding SiO_2, rather than from the Si substrate. From the density of nanocrystals and the inferred density of P_b defects, we estimate that there is, on average, 1 P_b defect every 1.4 nanocrystals, *i.e.* that at least 30% of the Si nanocrystals are P_b-defect free, and potentially optically active.

In a second step, the influence of ultra-violet (UV) irradiation on the defects in the sample was investigated. The sample was irradiated with UV light with a wavelength of 362 ± 20 nm for 71 hours, using a 150 W xenon arc-lamp and an interference filter. Subsequent to this, the filter was removed from the 150 W xenon arc-lamp, and the sample was irradiated with the full UV spectrum centered at 8.2 eV (180-1000 nm) for 10 hours. After each illumination step ESR was performed in order to determine the influence on the defects in the sample. As might be expected, signals from the SiO_2 specific centres E'_γ[25] and EX[26,27] were observed after irradiation with 362 nm UV light, and their intensity increased drastically after irradiation with the full UV spectrum (Fig. 3)[28]. On the other hand, the P_{b0} and P_{b1} signals did not change within the experimental error of ± 30 % after UV irradiation, indicating that there is no hydrogen passivation of the P_b centres in the as-crystallized sample, *i.e.* they are fully activated. This is consistent with the sample fabrication procedure which involves annealing at 1100°C in an N_2 atmosphere.

The ESR data demonstrate that the sample has a large number of different defects. None of the defects detected by ESR in the as-crystallized or even in the irradiated sample are PL-active. Nonetheless, this does not prove that the observed PL is from quantum confinement, and not from defects. Interface defects that are weakly observed or inactive in ESR can be present, and may even show a Si nanocrystal size dependence, as discussed in Refs 8,9,10,11. For example, Si/SiO_2 defect states which are close to the band edges of the Si nanocrystals,

and thus even follow the band-gap widening of Si due to quantum confinement have been reported[8]. In such defects, the PL is initiated by interband carrier excitation in the Si nanocrystals, followed by relaxation to the interface defect states (Fig. 4). The transition to the lower-energy interface defect state is radiative, with a PL energy close to the one determined from quantum confinement [8]. However, the aim here is not to identify the microscopic origin of interface-defect PL in Si/SiO_2, but to unambiguously demonstrate that we can distinguish between quantum confinement and defect PL in Si/SiO_2 nanostructures using a high magnetic field, and that we can switch between the two sources of PL in a single sample.

ORIGIN OF THE PHOTOLUMINESCENCE FROM AS-CRYSTALLIZED AND PASSIVATED NANOCRYSTALS

To determine the origin of the luminescence, PL measurements were performed at 85 K in pulsed magnetic fields, B, up to 50 T on the as-crystallized sample, *i.e.* prior to UV irradiation. The principle behind such experiments is quite straightforward: the applied magnetic field has an associated length scale, the magnetic length $\ell = \sqrt{\hbar/eB}$, where $\hbar$ is the reduced Planck constant and e is the electron charge, which acts to confine the wave function of the state under study prior to recombination, and hence increases the PL energy. Clearly, the smaller the extent of the wave function, the smaller the diamagnetic shift of the centre of mass of the PL, ΔE_{CM}. Indeed, in the low-field limit, where ℓ is large compared to the wave-function extent[18,19,29],

$$\Delta E_{CM} = \frac{e^2 \langle \rho^2 \rangle}{8\mu} B^2, \qquad (1)$$

where μ is the reduced effective mass and $\langle \rho^2 \rangle^{1/2}$ is the average wave-function extent in the plane perpendicular to the applied field. Thus, such an experiment should be able to

unequivocally distinguish between a state confined to a few nm's within a Si nanocrystal and a highly-localised defect state. However, such experiments are not trivial to perform in practice. The laser light and PL are transmitted to and from the magnet and cryostat using optical fibres, which also show a PL signal at a similar energy to that of the sample as a result of UV absorption in the fibres. This necessitates the use of special procedures to eliminate this background (see Methods section). Secondly, the sample signal is relatively weak compared with III-V semiconductor nanostructures, and requires the use of a state-of-the-art charge-coupled-device detector capable of single photon detection in order to count sufficient photons in the 5 ms integration time. For the same reason it was only possible to obtain a single spectrum at the peak field of each 25 ms magnetic-field pulse. Finally, the expected diamagnetic shift of the PL at 50 T is expected to be extremely small, even for quantum confinement: about 0.5% of the full width at half maximum of the PL (300 meV). In order to detect such small changes in the PL energy in an experiment that involves making a series of pulses for each field value over the period of a day, the zero-field peak position was measured before and after every pulse to eliminate any effects of drift over time in the apparatus, and to reduce the effects of heating from the pulse and mechanical realignment. As a result we define ΔE_{CM} as the difference in energy of the PL at the peak of the pulse and the average of the two zero-field values taken before and after the pulse. The result is plotted in Fig. 5a for the as-crystallized sample. It can be seen that the shift, if any, is very small. Since there is a slight hint of a very small shift, it is not possible to exclude a small contribution to the PL from quantum confinement. Nonetheless, it is clear that in the as-crystallized state the PL is completely dominated by PL from highly-localised defect states. This conclusion appears to contradict previous work that has cited the observation of phonon replica as proof of quantum confinement in ensemble studies of samples similar to those studied here[30]. On the other hand, in single dot measurements of Si nanocrystals formed in etched nanopillars[31], an acoustic

phonon replica at 6 meV was always observed, whereas optical phonon replica were only observed for ~1/3 of the dots. This was noted as being somewhat unexpected, and tentatively attributed to the carriers being 'strongly localised' in some nanocrystals. (A highly localised state has a small dipole and so will couple weakly to optical phonons.) Clearly, the question of phonon replica associated with defect states needs further investigation.

In the next step, we passivated the sample in 1 atmosphere of pure hydrogen for 30 minutes at a temperature of 400°C. This temperature does not influence the size and nature of the Si nanocrystals since the formation of amorphous Si clusters needs temperatures in excess of 600°C, and crystallization of amorphous Si clusters only appears above 900°C[32]. We then repeated the ESR and PL measurements. The zero-field PL and ESR spectra are shown in Figs. 2 and 6a respectively. Firstly, it can be seen that the passivation has had a remarkable effect on the ESR signal (Fig. 6a). All traces of any defects have been removed: the only part that remains being the Si:P marker signal. Secondly, the intensity of the PL signal has increased, consistent with the removal of the P_b defects. Assuming that the passivation has also eliminated the ESR-inactive defects, we can suppose that the PL is now of entirely quantum-confinement origin. This can be clearly seen in the data from a second magneto-PL experiment (Fig. 5b): A parabolic shift of about 1.5 meV is observed. Using an estimated reduced mass of 0.20 m_0 (m_0 is the free electron mass), obtained by assuming an isotropic electron mass of 0.33 m_0 and a heavy hole mass of 0.54 m_0[33], a wave-function extent of 4.9 ± 0.1 nm in the plane of the sample is found. This is somewhat bigger than the diameter of 3 nm measured from high-resolution TEM, and may result from the fact that the transition from Si to SiO_2 occurs through a sub-oxide layer, resulting in some leakage of the confined wave-function out of the nanocrystal[22].

Doi:10.1038/nnano.2008.7

RE-INTRODUCING THE DEFECTS

Having demonstrated the origin of the PL as defects in the as-crystallized state and quantum confinement after passivation, we then went on to reintroduce the defects using UV illumination from an Ar^+ laser (351 to 364 nm radiation). Two experiments were conducted. Firstly, the whole surface of a piece of passivated sample was irradiated at room temperature by a defocused beam for almost 330 hours. The effect on the ESR spectrum is shown in Fig. 6a. The irradiation has reactivated the P_b and E'_γ centres, although the density of defects is substantially less than for the as-crystallized sample. In the second experiment another piece of passivated sample was irradiated at room temperature by an unfocused Ar^+ laser beam over a period of 8 hours, and PL spectra were taken at regular intervals. It is estimated that the accumulated doses of UV radiation received in the two experiments is similar, but our conclusions are not dependent on the two treatments being equivalent. The integrated intensity and centre of mass of the PL are shown in Fig. 6b as a function of irradiation time with the unfocused laser beam. It can be seen that both curves have a 'fast' and a 'slow' component. The intensity initially rapidly increases, and then after about two hours starts to decrease. The centre of mass shows a strong red-shift, followed by a weaker dependence after the same two hour period. Indeed, both curves can be fitted with a double exponential function, yielding the same two timeconstants in both cases: 26 minutes for the 'fast' component and 337 minutes for the 'slow' component. This implies that the observed behaviour is the result of two competing effects. Since we know from ESR that UV illumination introduces or reactivates defects due to the Stæbler-Wronski effect[34], we attribute the first mechanism, which *increases* the PL intensity, to the reactivation of the interface defects responsible for the PL in the as-crystallized sample. This explanation is consistent with the observed red-shift, since such defects emit PL at an energy that is slightly lower than that of quantum confinement[8]. For the same reason we can expect that the reactivation of the

defect PL in any particular nanocrystal will quench the quantum confinement PL, especially if carrier relaxation from the Si conduction band to interface defect states (Fig. 4) is faster than the recombination time. The second effect, with a much slower timeconstant, decreases the PL intensity, and is therefore very likely to be the result of the reactivation of P_b defects in the Si nanocrystals, since they quench the PL and are known to reappear as a result of illumination with the UV lines of the Ar^+ laser [Fig. 6a]. The corresponding red shift of the PL can be attributed to the preferential reactivation of defects in smaller nanocrystals that emit at higher energies, as these will tend to be more strained. The net effect is that illumination with UV light reverses the effect of passivation, and we return to interface defects as the origin of the PL. Note that H is immobile in the sample at 85 K, thus the UV illumination during the magneto-PL experiments does not affect the defects.

Since the timeconstant of the fast component in Fig. 6b is 26 minutes, illumination for 8 hours should result in 95% of the interface defects being reactivated. Although their PL may still be quenched by the reintroduction of P_b-type defects, we can reasonably expect that after illumination the PL is, once again, totally of interface-defect origin. Fig. 5c shows ΔE_{CM} versus magnetic field for the sample that was passivated and subsequently irradiated with a defocused laser beam. Although the data is somewhat noisy, it is evident that there is no diamagnetic shift, entirely confirming our expectations: the PL is of defect-related origin again.

In summary, we have shown that high magnetic fields can be used to unambiguously classify the origin of photoluminescence from Si nanocrystals in SiO_2 as either from defects or quantum confinement. We have further shown that by a combination of passivation to remove defects and UV irradiation to reintroduce them, we can switch from defect-related photoluminescence, to quantum-confinement photoluminescence and back again to defect-related photoluminescence in a single sample.

Doi:10.1038/nnano.2008.7

Methods

SUPERLATTICE APPROACH

An amorphous SiO/SiO_2 superlattice is grown by reactive evaporation of SiO powders in an oxygen atmosphere. The films were deposited on 4 inch wafers with a substrate temperature of 100°C. Rotation of the substrate enables a high homogeneity over the whole wafer. The Si nanocrystals are then formed by phase separation during thermal annealing at 1100°C for one hour under N_2 atmosphere: $2\ SiO \rightarrow SiO_2 + Si$. This growth method allows the independent control of crystal size and density, and the Si nanocrystals are separated by a thin oxide shell[21].

ELECTRON SPIN RESONANCE

Conventional first-order absorption-derivative (dP_μ/dB) ESR is measured using a K-band spectrometer operating at a frequency of ~ 20.5 GHz, equipped with a TE_{011} cavity. For reasons of sensitivity, all spectra were taken at 4.2 K. The measurements were performed with the amplitude of the applied sinusoidal modulation of the magnetic field (~ 100 kHz) and incident microwave power properly adjusted so that the measured signals were not visibly distorted. In order to improve the signal-to-noise ratio for each spectrum typically 100 scans were accumulated. For ESR signal intensity and g factor calibration, a Si:P marker sample was identically co-mounted with the Si nanocrystal sample for each measurement. To get the absolute values of the defect densities, the double numerical integration of the detected derivative absorption spectrum was compared with that of the marker, both recorded in the same trace. Generally, measurements were carried out with the applied magnetic field $\vec{B} \parallel \vec{n}$, the (100) Si substrate normal. The signal anisotropy was checked by varying the angle (φ_B) $\vec{B}$ makes with $\vec{n}$.

Doi:10.1038/nnano.2008.7

PHOTOLUMINESCENCE IN PULSED MAGNETIC FIELDS

To conduct PL measurements in high magnetic fields, optical fibres are used to bring the laser light to the sample. For the measurements discussed here, a long (25 m) and a short (2 m) excitation fibre were used with a band pass filter in between. The emitted light was transferred to the detector via a bundle of 7 detection fibres 25 m in length. Because of the low PL intensity, an exposure time of 5 ms was needed and only one spectrum could be taken during a 25 ms magnetic field pulse. The exposure time was chosen at the peak of the pulse in such a way that the standard deviation of the magnetic field while counting photons was less than 5 %. The plane of the sample was mounted at an angle of 8° to the plane perpendicular to the applied field, and the excitation fibre was placed at an angle of 11° with respect to the collection fibres, which were parallel to the applied field, in such a way as to make an angle of 19° between the laser excitation and PL detection fibres. This was done to reduce the reflection of the UV laser light into the detection fibres. Further details on the magneto-PL technique and its application to semiconductor nanostructures can be found in Ref 19.

Doi:10.1038/nnano.2008.7

Acknowledgements

This work was supported by the SANDiE Network of Excellence of the European Commission (NMP-CT-2004-500101), the Belgian Inter-university Attraction Pole, Flemish Geconcerteerde Onderzoeksacties and Fonds voor Wetenschappelijke Onderzoek programmes and project ZA191/14-3 of the German Research Foundation (DFG). M.H. is an Academic Fellow of the Research Councils UK. Correspondence and requests for materials should be addressed to M.H.

Competing Financial Interests

The authors declare no competing financial interests.

[1] Ball, P. Let there be light. *Nature* **409**, 974-976 (2001).

[2] Canham, L. T. Silicon quantum wire array fabrication by electrochemical and chemical dissolution of wafers. *Appl. Phys. Lett.* **57,** 1046-1048 (1990).

[3] Lehmann , V. & Gösele, U. Porous Si formation: A quantum wire effect. *Appl. Phys. Lett.* **58,** 856-858 (11991).

[4] Fauchet, P.M., Photoluminescence and electroluminescence from porous silicon, *J. Lumin.* **70**, 294-309 (1996).

[5] Wolkin, M.V. *et al.*, Electronic states and luminescence in porous Si: The role of oxygen. *Phys. Rev. Lett.* **82**, 197-200 (1999).

[6] Hadjisavvas, G & Kelires, P.C. Theory of interface structure, energetics, and electronic properties of embedded Si/a-SiO_2 nanocrystals. *Physica E* **38**, 99-105 (2007).

[7] Heitmann, J., Müller, F., Zacharias, M. & Gösele, U. Silicon nanocrystals: Size matters. *Adv. Mater* **17**, 795-803 (2005).

[8] Averboukh, B. *et al.* Luminescence studies of a Si/SiO_2 superlattice *J. Appl. Phys.* **92**, 3564-3568 (2002).

[9] Puzder, A., Williamson, A.J., Grossman, J.C. & Galli, G. Surface Chemistry of Silicon Nanoclusters, *Phys. Rev. Lett.* **88**, 097401 (2002).

[10] Hadjisavvas, G & Kelires, P.C. Structure and Energetics of Si Nanocrystals Embedded in *a*-SiO_2, *Phys. Rev. Lett.* **93**, 226104 (2004).

[11] Wang, X.X. *et al.* Origin and evolution of photoluminescence from Si nanocrystals embedded in a SiO_2 matrix, *Phys. Rev. B* **72**, 195313 (2005).

[12] Pavesi, L., Dal Negro, L., Mazzoleni, C., Franzo, G. & Priolo, F. Optical gain in silicon nanocrystals. *Nature* **408**, 440-444 (2000).

[13] Walters, R. J., Bourianoff, G. I. & Atwater, H. A. Field-effect electroluminescence in silicon nanocrystals, *Nat. mater.* **4**, 143-146 (2005).

[14] Tiwari, S. *et al.* A silicon nanocrystal based memory. *Appl. Phys. Lett.* **68,** 1377-1379 (1996).

[15] Delerue, C., Allan, G. & Lannoo, M. Theoretical aspects of the luminescence of porous silicon. *Phys. Rev. B* **48,** 11024-11036 (1993).

[16] Delley, B. & Steigmeier, E. F. Quantum confinement in Si nanocrystals. *Phys. Rev. B* **47,** 1397-14000 (1993).

[17] Ogüt, S., Chelikowsky, J. R. & Louie, S. G. Quantum confinement and optical gaps in Si nanocrystals. *Phys. Rev. Lett.* **79,** 1770-1773 (1997).

[18] Hayne, M. *et al.* Electron and hole confinement in stacked self-assembled InP quantum dots. *Phys. Rev. B* **62,** 10324-10328 (2000).

[19] Hayne, M. *et al.* Pulsed magnetic fields as probe of self-assembled semiconductor nanostructures. *Physica B* **346-347**, 421-427 (2004).

[20] Poindexter, E. H. & Caplan, P. J. Characterization of Si/SiO_2 interface defects by electron spin resonance. *Prog. Surf. Sci.* **14,** 201-294 (1983).

[21] Zacharias, M. *et al.* Size-controlled highly luminescent silicon nanocrystals: A SiO/SiO_2 superlattice approach. *Appl. Phys. Lett.* **80,** 661-663 (2002).

[22] Zimina, A *et al.* Electronic structure and chemical environment of silicon nanoclusters embedded in a silicon dioxide matrix Appl. Phys. Lett. **88**, 163103 (2006).

[23] Stesmans, A. & Afanas'ev, V. V. Electron spin resonance features of interface defects in thermal $(100)Si/SiO_2$. *J. Appl. Phys.* **83,** 2449-2457 (1998).

[24] Stesmans, A., Nouwen, B. & Afanas'ev V. V. P_{b1} interface defect in thermal $(100)Si/SiO_2$: ^{17}Si hyperfine interaction. *Phys. Rev. B* **58,** 15801-15809 (1998).

[25] Warren, W. L., Poindexter, E. H., Offenberg, M. & Müller-Warmuth, W. Paramagnetic point defects in amorphous silicon dioxide and amorphous silicon nitride thin films. *J. Electrochem. Soc.* **139,** 872-880 (1992)

[26] Stesmans, A. & Scheerlinck, F. Generation aspects of the delocalized intrinsic EX defect in thermal SiO_2. *J. Appl. Phys.* **75,** 1047-1058 (1994).

[27] Stesmans, A. & Scheerlinck, F. Natural intrinsic EX center in thermal SiO_2 on Si: ^{17}O hyperfine interaction. *Phys. Rev. B* **50,** 5204-5212 (1994).

[28] Tsai, T. E., Griscom, D. L., Friebele & E. J. Mechanism of intrinsic Si E'-center photogeneration in high-purity silica. *Phys. Rev. Lett.* **61,** 444-446 (1988).

[29] Walck, S.N. & Reinecke, T.L. Exciton diamagnetic shift in semiconductor nanostrucures. Phys. Rev. B **57**, 9088-9096 (1998).

[30]Heitmann, J., Müller, F., Yi., L., Zacharias, M., Kovalev, D. & Eichhorn, F. Excitons in Si nanocrystals: Confinement and migration effects. *Phys. Rev. B* **69**, 195309 (2004).

[31] Sychugov, I., Juhasz, R., Valenta, J. & Linnros, J. Narrow luminescence linewidth of a silicon quantum dot. *Phys. Rev. Lett.* **94**, 087405 (2005).

Doi:10.1038/nnano.2008.7

---

[32] Yi, L. X., Heitmann, J., Scholz, R. & Zacharias, M. Si rings, Si clusters, and Si nanocrystals - different states of ultrathin SiO_x layers. *Appl. Phys. Lett.* **81,** 4248-4250 (2002).

[33] Davies, J. H. *The physics of low-dimensional semiconductors*, (Cambridge University Press, Cambridge, UK, 1998).

[34] Abtew, T. A. & Drabold, D. A. Atomistic simulation of light-induced changes in hydrogenated amorphous Si. *J. Phys.: Cond. Mat.* **18**, L1-L6 (2006).

Doi:10.1038/nnano.2008.7

Figure 1 Imaging of Si nanoparticles by high resolution transmission electron microscopy (HRTEM). a Image of a single Si nanoparticle along the [011] zone axis; **b** corresponding Fourier transform; **c** Bragg-filtered HRTEM image and **d** Bragg filtered image after subtraction of the background. The latter clearly highlights the {111} faceting of this nanoparticle.

Figure 2 Room temperature PL spectra. The spectra were taken under the same experimental conditions for the sample in its as-crystallised (blue line) and passivated (red line) states.

Figure 3 ESR spectra at 4.2 K The upper spectrum is in the as-crystallized state, the middle spectrum after xenon arc-lamp illumination at ~ 362 nm, and the lower spectrum after unfiltered xenon arc-lamp irradiation. In total four different defects are identified: P_{b0}, P_{b1}, E'_{γ} and EX, which are also schematically represented. The purple and green spheres represent the Si and O atoms respectively. The arrows depict the unpaired electrons and the brown Si-Si bond indicates the strained bond. The signal Si:P is a marker from an added reference sample.

Figure 4 Schematic representation of the band structure of Si nanocrystals embedded in SiO_2 with the competing PL mechanisms (adapted from Ref. 8). The band gap of SiO_2 is 8.8 eV while the band gap of Si has increased from 1.12 eV (bulk) to 1.6 - 2.6 eV for the Si nanocrystals due to quantum confinement (QC). There are two different bands of defect states: the interface defect states close to the conduction band of Si and the mid-gap defect states with energies close to the valence band of Si. The conduction band of the Si nanocrystal has two sub-levels as explained in Ref. 8.

Doi:10.1038/nnano.2008.7

Figure 5 Shift of the centre of mass of the PL peak (ΔE_{CM}) as a function of magnetic field at 85 K. The error bars are the mean of the absolute difference in centre of mass of 0 T spectra taken before and after each field pulse. **a** Data for the as-crystallised sample. The dotted line indicates the mean value of ΔE_{CM}. **b** After passivation. The solid line shows the parabolic fit. **c** After passivation and subsequent UV irradiation at room temperature. The dotted line is the mean value. A clear parabolic field dependence, such as is observed in **b,** is characteristic of a PL from a state that is quantum confined by the nanocrystal, whereas no detectable field dependence indicates that a very highly localised (defect) state is responsible for the PL (**a** and **c**). The error bars in **b** are much smaller than in **a** or **c** due to the increased intensity of the signal.

Figure 6: Effect of UV irradiation on a passivated sample. a ESR spectra at 4.2 K for the passivated sample (upper spectrum) and after subsequent UV irradiation (lower spectrum). It can be seen that passivation removes the defects (the only remaining signal is the Si:P marker), and that UV irradiation re-introduces them. **b** Time dependence of the centre of mass (left-hand axis) and integrated intensity (right-hand axis) of the PL, after passivation and during irradiation with the UV lines of an unfocused Ar^+ laser. The lines are fits to the data using double exponential functions.

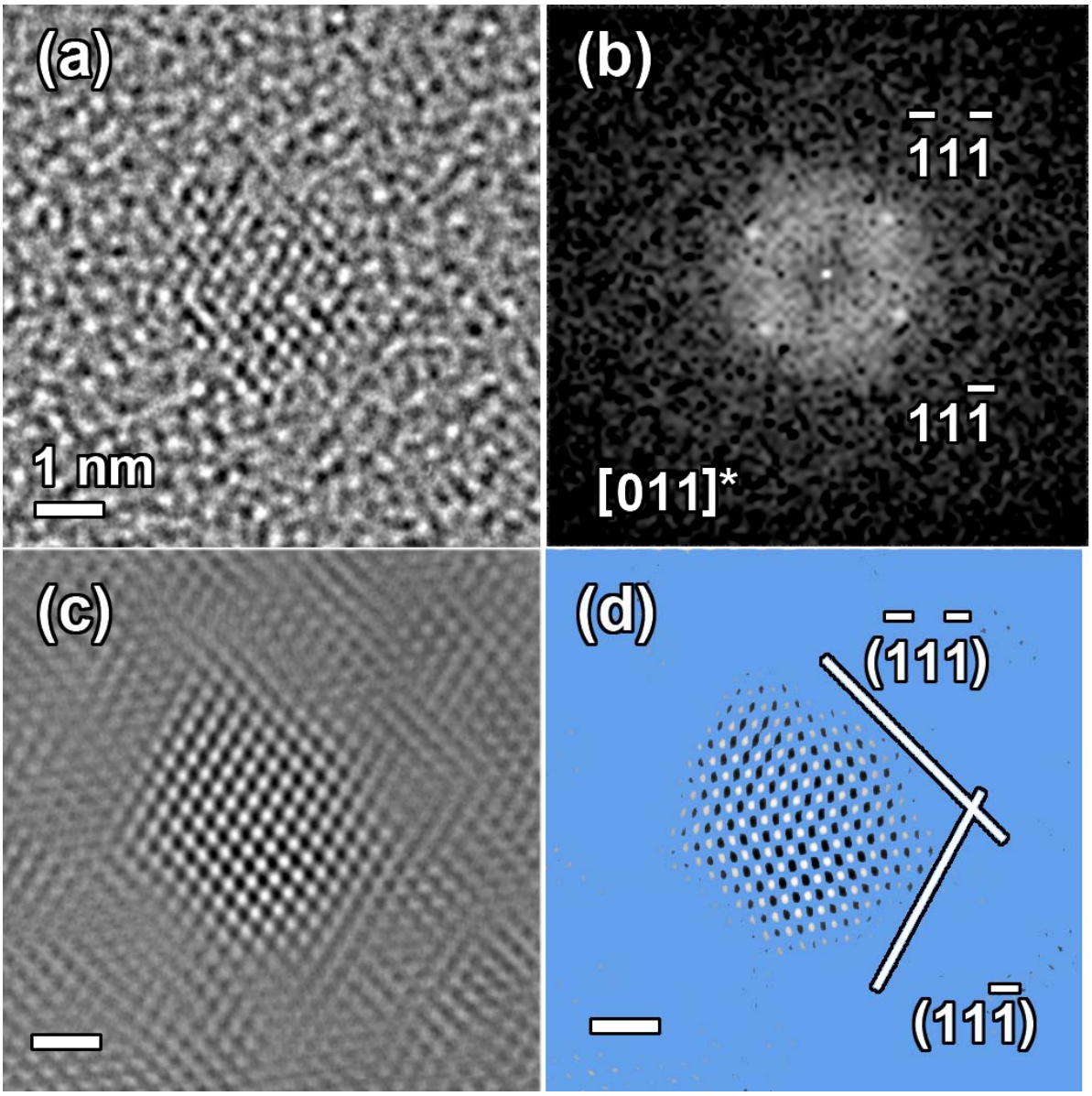

Figure 1

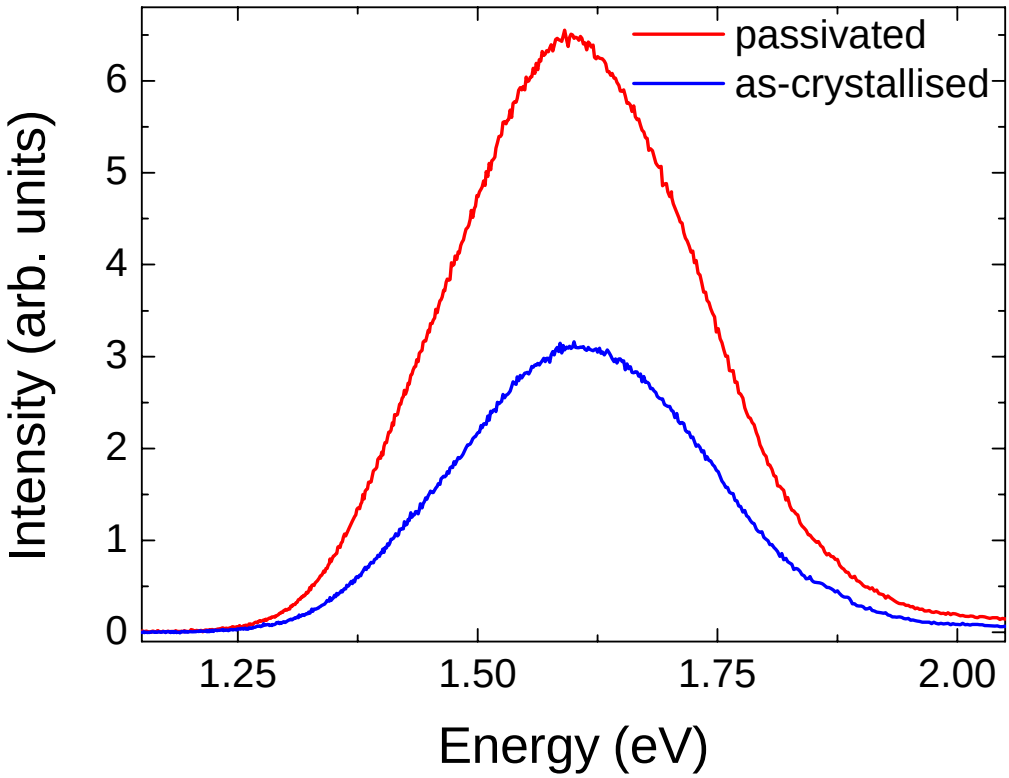
passivated
as-crystallised
Intensity (arb. units)
0
1
2
3
4
5
6
1.25
1.50
1.75
2.00
Energy (eV)

Figure 2

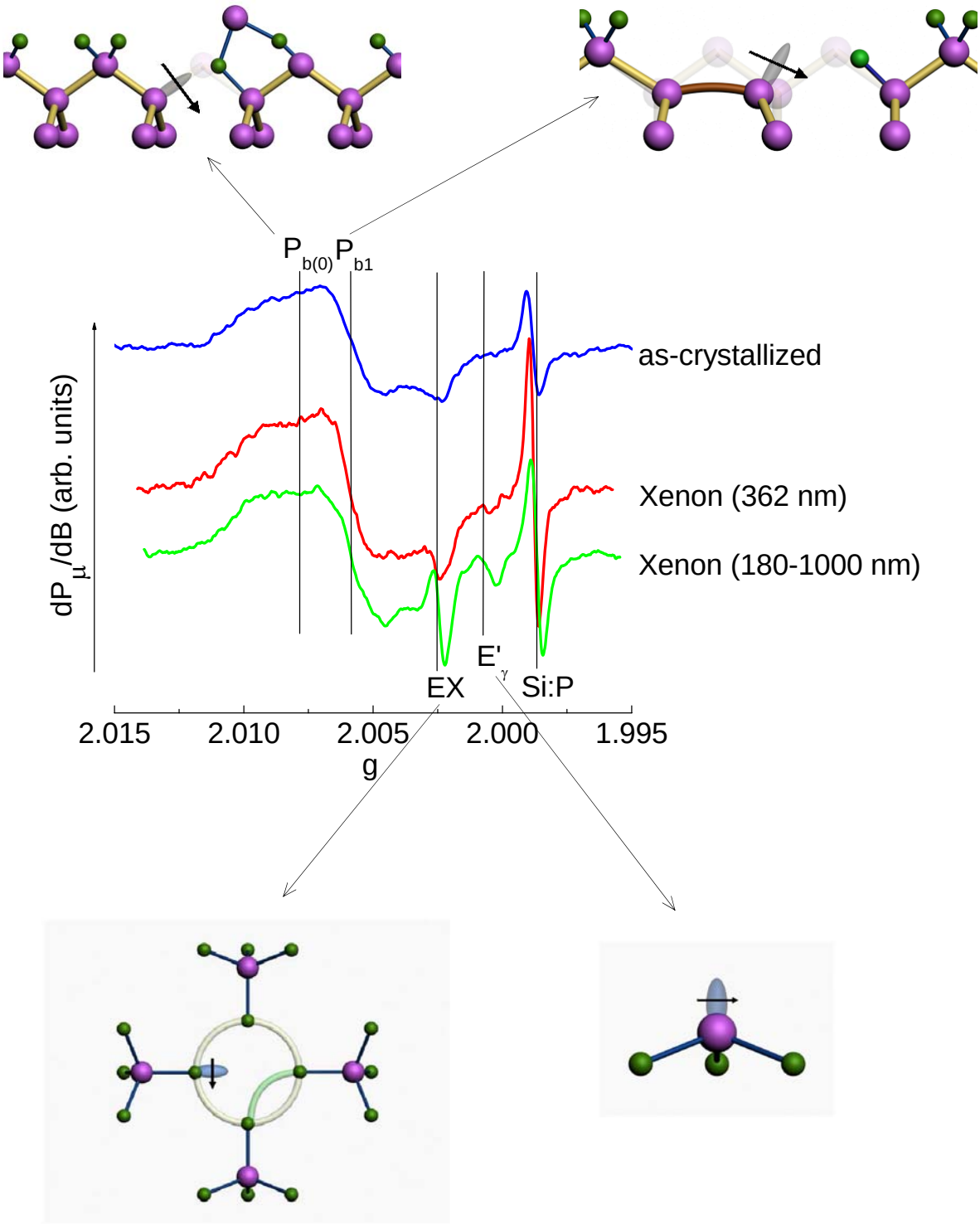
P b(0) P b1
as-crystallized
Xenon (362 nm)
Xenon (180-1000 nm)
dP μ /dB (arb. units)
E' γ
EX
Si:P
2.015
2.010
2.005
2.000
1.995
g

Figure 3

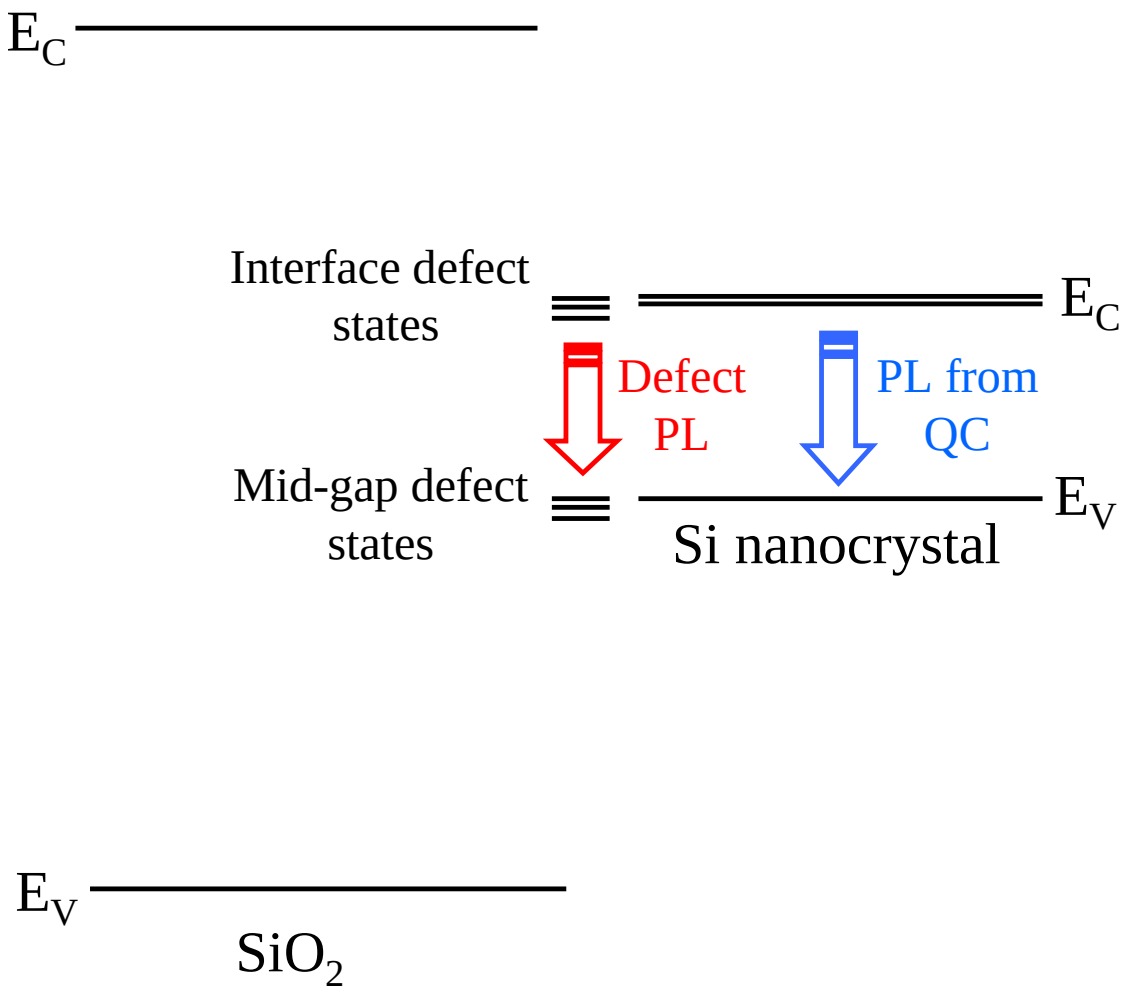
E_C
Interface defect states
E_C
Defect PL
PL from QC
Mid-gap defect states
E_V
Si nanocrystal
E_V
SiO_2

Figure 4

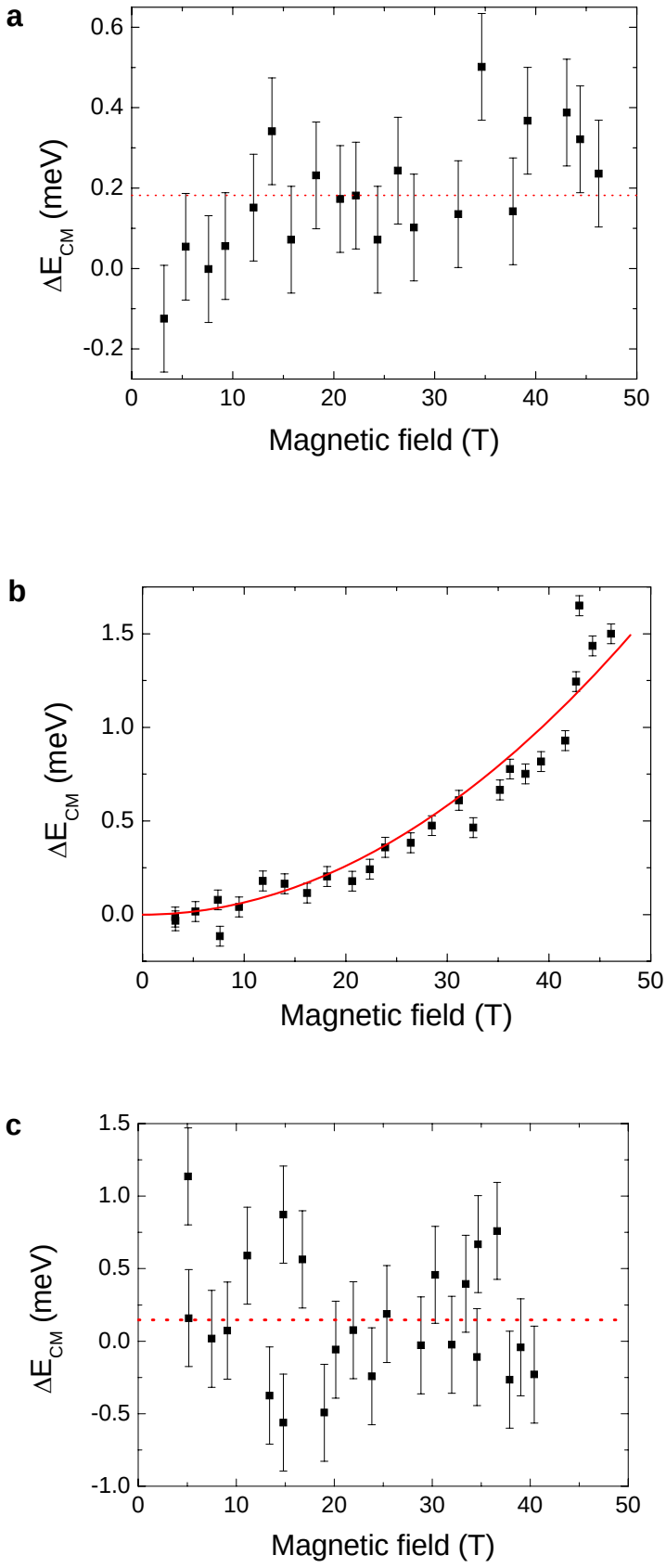
a
0.6
0.4
0.2
0.0
-0.2
ΔE_CM (meV)
0
10
20
30
40
50
Magnetic field (T)
b
1.5
1.0
0.5
0.0
ΔE_CM (meV)
0
10
20
30
40
50
Magnetic field (T)
c
1.5
1.0
0.5
0.0
-0.5
-1.0
ΔE_CM (meV)
0
10
20
30
40
50
Magnetic field (T)

Figure 5

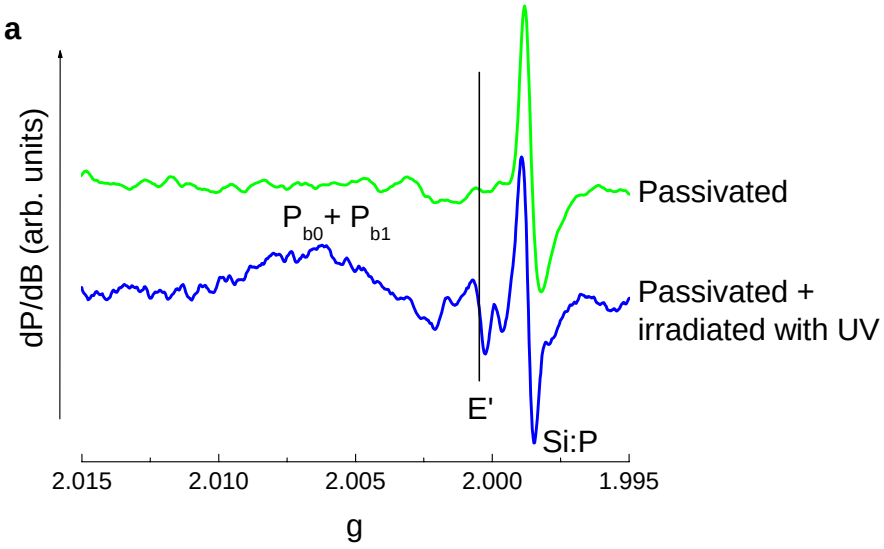
a
dP/dB (arb. units)
Passivated
P b0 + P b1
Passivated +
irradiated with UV
E'
Si:P
2.015
2.010
2.005
2.000
1.995
g

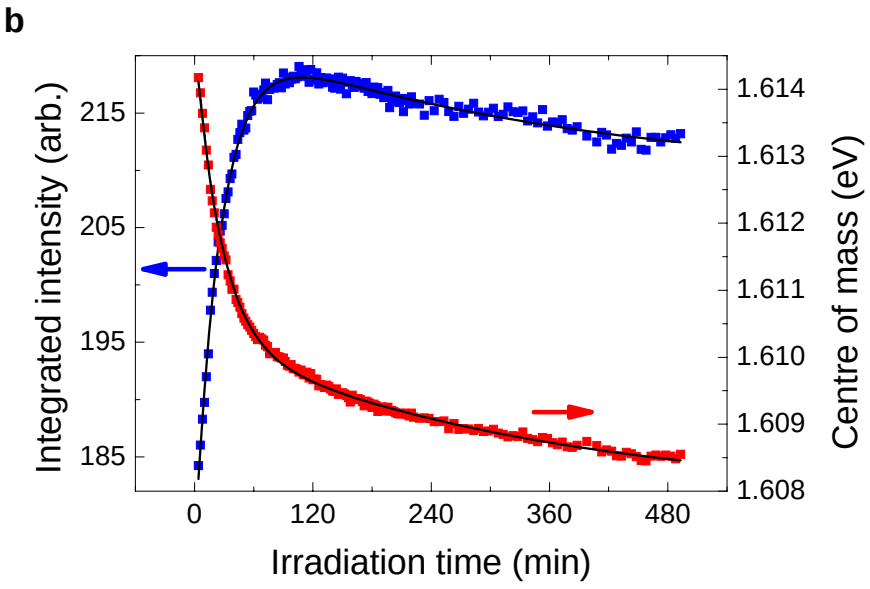
b
Integrated intensity (arb.)
215
205
195
185
1.614
1.613
1.612
1.611
1.610
1.609
1.608
Centre of mass (eV)
0
120
240
360
480
Irradiation time (min)

Figure 6